Available online at www.sciencedirect.com
ScienceDirect
Journal of Non-Crystalline Solids 352 (2006) 3872–3878
JOURNAL OF NON-CRYSTALLINE SOLIDS
www.elsevier.com/locate/jnoncrysol

Deformation behaviors of a tungsten-wire/bulk metallic glass matrix composite in a wide strain rate range

G. Wang [a,b], D.M. Chen [c], J. Shen [a,*], Z.H. Stachurski [d], Q.H. Qin [d], J.F. Sun [a], B.D. Zhou [a]

[a] School of Materials Science and Engineering, Harbin Institute of Technology, 92 West Dazhi Street, Harbin 150001, China
[b] Institute of Physics, Chinese Academy of Sciences, Beijing 100080, China
[c] Department of Mechanical Engineering, Academy of Armoured Forces Engineering College, Beijing 100072, China
[d] Department of Engineering, FEIT, The Australian National University, ACT 0200, Australia

Received 29 September 2005; received in revised form 31 May 2006
Available online 1 September 2006

Abstract

Using melt infiltration casting a composite (W-BMG) of $Zr_{41.25}Ti_{13.75}Ni_{10}Cu_{12.5}Be_{22.5}$ bulk metallic glass reinforced with tungsten wires has been produced and its quasi-static and dynamic deformations are investigated within the strain rates ranging from 1×10^{-4} to $2 \times 10^{3}\ s^{-1}$. The lengthwise frozen-in stress of the composite during the fabrication process is also calculated. The quasi-static stress–strain behavior is discussed in detail in light of the observation of the appearances of the specimens. The study reveals that the strain rate sensitivity exponent of 0.022 of the W-BMG composite is half that of the monolithic tungsten, which is a result of the frozen-in stress.

PACS: 62.20.Fe; 62.20.Dc

Keywords: Amorphous metals; Metallic glasses; Alloys; Metal-matrix composites; Strength

1. Introduction

Bulk metallic glasses (BMGs) have shown a great potential to be used as structural materials due to their unique properties such as extremely high strength, high hardness and good toughness [1–5]. However, monolithic BMGs always fail catastrophically along narrow shear bands when loaded in tension or compression. They usually exhibit very limited plasticity before fracture. The development of BMG matrix composites opens new prospects for application of BMGs in modern industries [6–10]. Unlike monolithic BMGs, these composites can undergo substantial plastic deformation in compression [11–13]. Among various BMGs, $Zr_{41.25}Ti_{13.75}Ni_{10}Cu_{12.5}Be_{22.5}$ BMG has received the most attentions for its superior glass forming ability and mechanical properties [14,15]. Especially, owning to its desirable properties including localized shear bands (resulting in self-sharpening behavior) and the high density, $Zr_{41.25}Ti_{13.75}Ni_{10}Cu_{12.5}Be_{22.5}$ BMG composite enhanced by tungsten wires has attracted widespread attention [11] which leads to important applications in the field of engineering materials such as kinetic energy penetrators and some engineering materials subjected to a dynamic deformation condition [6,11,16]. In general, split Hopkinson pressure bar (SHPB) is a usual technique to investigate materials' deformation behavior under high strain rate condition [17–21]. So far, although ballistic tests have been used to study the dynamic deformation of the BMG composites [6,16], SHPB technique has not been employed to investigate the deformation behavior of the W-BMG composite. In this paper, we study the compressive deformation behaviors of the tungsten wires-$Zr_{41.25}Ti_{13.75}Ni_{10}$-

* Corresponding author. Tel.: +86 451 86418317; fax: +86 451 86473903.
E-mail address: junshen@hit.edu.cn (J. Shen).

0022-3093/$ - see front matter
doi:10.1016/j.jnoncrysol.2006.06.037

$Cu_{12.5}Be_{22.5}$ BMG composite both under the quasi-static condition and under the high strain rate condition.

2. Experimental process

In this section details of the experimental procedure and the dimensions of the specimens are described. $Zr_{41.25}Ti_{13.75}Ni_{10}Cu_{12.5}Be_{22.5}$ alloy ingots were prepared by arc melting a mixture of pure metal elements in a titanium-gettered argon atmosphere followed by suction into a copper mould to form BMG rod samples with a diameter of 5 mm and a length of 70 mm. Unidirectional tungsten wires with a diameter of 1 mm were then cut into 70 mm (length) and degreased by ultrasonic cleaning in a bath of acetone followed by the same procedure in a bath of ethanol. The melt infiltration casting [22] was used to manufacture the W-BMG composite. A schematic drawing of the apparatus is shown in Fig. 1. The tungsten wires were placed in the sealed end of a quartz tube with an inner diameter of 7 mm. A necked tube was set up about 10 mm above the tungsten wires, and then the BMG ingot was inserted in the tube above the neck. The necked tube is necessary to minimize premature contact between the BMG melt and the tungsten wires to prevent excessive reaction. Prior to heating, the tube was evacuated and then purged with argon gas. The assembly of tube was heated to approximately 1127 K, which is higher than the liquidus temperature of the BMG, and then held for 10 min to allow the BMG to melt completely. After that, the argon gas with a positive pressure of 0.24 MPa was applied to push the BMG melt to infiltrate through the bundle of the tungsten wires and the pressure was maintained for 20 min. Then the assembly of tube was quickly removed from the furnace and quenched in brine (8 wt% $NaCl/H_2O$ solution). The W-BMG composite samples have a dimension of ϕ 7×60 mm and contain 68% tungsten wires by volume fraction. For reference, ideal close packing of parallel rods reaches volume fraction close to 91%.

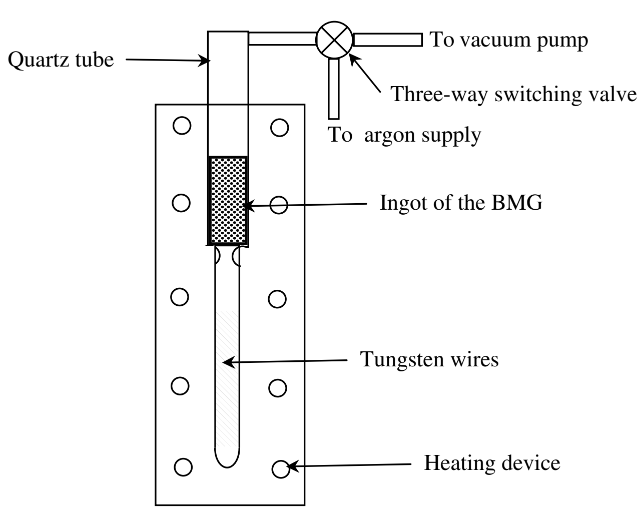

Fig. 1. Skeleton drawing of the set-up for melt infiltration casting.

The W-BMG specimens with a dimension of $\phi 7 \times 14$ mm and the BMG specimens with a dimension of ϕ 5×10 mm for compressive tests were fabricated by means of electrical discharge machining. These specimens were then used to perform quasi-static compressive tests under an Instron 5500R1186 machine with the strain rates ranging from 1×10^{-4} to 8×10^{-3} s^{-1} and dynamic compressive tests with a SHPB machine at a dynamic strain rate of 2×10^3 s^{-1}. The principal of the SHPB test has been described in Ref. [21]. A digital camera and a micrometer were used to record the appearances and dimensions of the specimens subjected to quasi-static compressive tests, respectively. The microstructure of the as-prepared W-BMG composite was observed by scanning electron microscope (SEM). The SEM observations were performed on a Cambridge STEREOSCAN 360 SEM to examine the as-prepared structure of the composite.

3. Results

3.1. Structure determination

The compactability of the W-BMG composite can be observed in Fig. 2 which shows the SEM cross-section micrographs of the W-BMG composite. The cross-section shows nearly close packed tungsten wires in the BMG matrix [see Fig. 2(a)]. A higher magnification of the

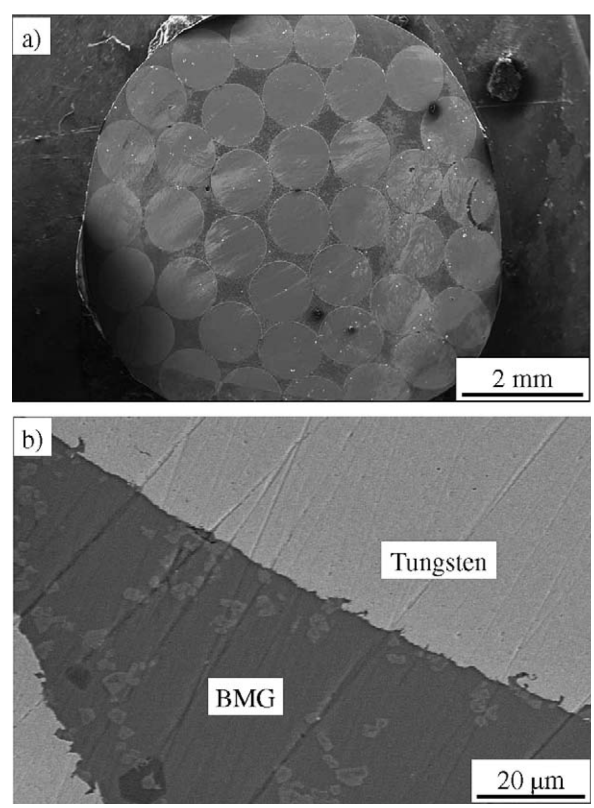

Fig. 2. Back scattered SEM images of the W–BMG composite. (a) cross-section micrograph; (b) interface micrograph between the tungsten wire and the BMG matrix.

interfacial region between the tungsten wire and the BMG matrix is shown in Fig. 2(b), from which some particles with grey contrast can be observed to be dispersed in the BMG matrix. These observations indicate that some crystalline phases precipitate from the BMG matrix, which were also reported in [7]. The volume fraction of the crystalline phase is estimated to be approximately 21%. The crystalline phase is likely to be Zr_2Cu according to energy dispersive X-ray (EDX) spectrum analysis and our previous experiments [23].

3.2. Compressive deformations

Quasi-static compressive tests were carried out on both monolithic BMG and W-BMG composite samples, repeated five times to exclude occasional effects in stress–strain behavior. As shown in Fig. 3, the monolithic BMG shows a perfect elastic deformation when the strain is less than 0.021, followed by a yielding plateau until the plastic strain reaches 0.03. The yield strength and fracture strength of the monolithic BMG are found to be 1817 and 1880 MPa, respectively. It is also found from Fig. 3 that the W-BMG composite shows a different stress–strain behavior exhibiting a much wider yielding plateau. The yield stress of the W-BMG composite of 1087 MPa is much lower than that of the pure BMG. The Young's modulus of the composite is 312 GPa, whereas Young's modulus of the BMG is 96 GPa. As the stress increases to 1817 MPa, the stress–strain curve shows a yielding plateau. With further increase of plastic strain, a weak strain hardening appears. The stress slightly increases to a maximum value of 2003 MPa and then fracture occurs. The maximum strain values of the monolithic BMG and the W-BMG composite are 0.03 and 0.14, respectively. The quasi-static compressive tests confirm that, although the tungsten reinforcement does not improve the strength, the plastic strain is promoted more than four times as compared with that of the monolithic BMG.

The dynamic compressive tests for the W-BMG were carried out at a strain rate of $2 \times 10^3\ s^{-1}$ and the measurements were repeated ten times to minimize random effects. A representative dynamic compressive stress–strain curve is shown in Fig. 4. Typically, in all dynamic tests a yield peak appears before general yielding, i.e., the stress increases at first to 2700 ± 44 MPa and then reduces to 2660 ± 38 MPa along with a small increase in strain. The initial 'elastic' deformation stage of the stress–strain curve shows a nonlinear behavior because SHPB is known to have some system errors [18]. When the stress drops to 2660 ± 38 MPa, a stress plateau appears. As the strain approaches approximately 0.04, the stress drops abruptly. Compared with the quasi-static compressive deformation, the dynamic compressive deformation of the W-BMG composite shows a higher compressive strength, a lower plastic strain and a distinct yield peak on the stress–strain curve.

3.3. Damage modes

To understand the effect of quasi-static load on deformation behavior of W-BMG composite, observation of the specimen appearances during the compressive deformation was carried out. The appearances corresponding to the deformation stages A, B and C, as indicated in the stress–strain curve [see Fig. 5(a)], are shown in Figs. 5(b), (c) and (d), respectively. In stage A, the deformation exhibits elastic behavior. The appearance and dimension of the specimen do not change with the removal of the load [see Fig. 5(b)]. When the strain reaches the yielding plateau, i.e., stage B, the stress–strain behavior shows an appreciable plastic strain, yet the specimen does not show any obvious difference in its appearance [see Fig. 5(c)]. Although the gauge length of the specimen deformed at stage B is slightly shortened, buckling of the tungsten wires does not occur on macroscale. Further observing the cross-section of the specimen deformed in stage B by SEM, many microcracks

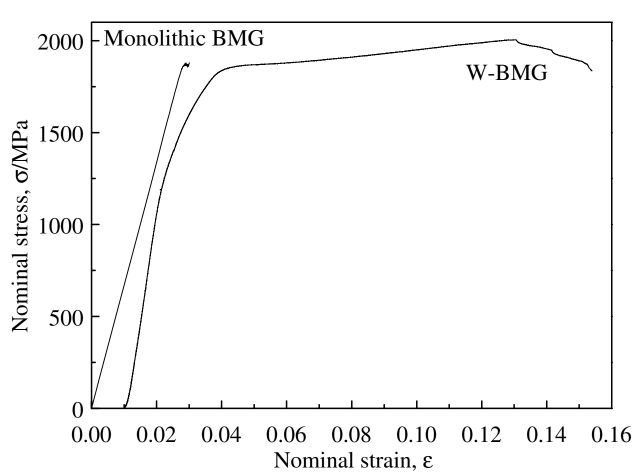

Fig. 3. Quasi-static compressive stress–strain behaviors of the monolithic BMG and the W–BMG composite.

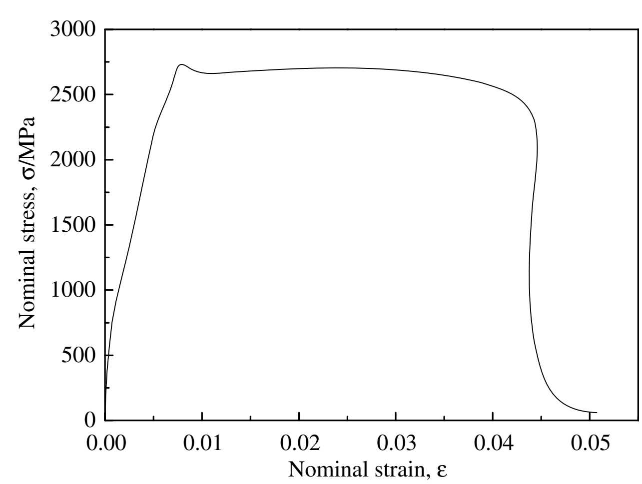

Fig. 4. Dynamic compressive stress–strain curve of the W–BMG composite ($\dot{\varepsilon} = 2 \times 10^3 s^{-1}$).

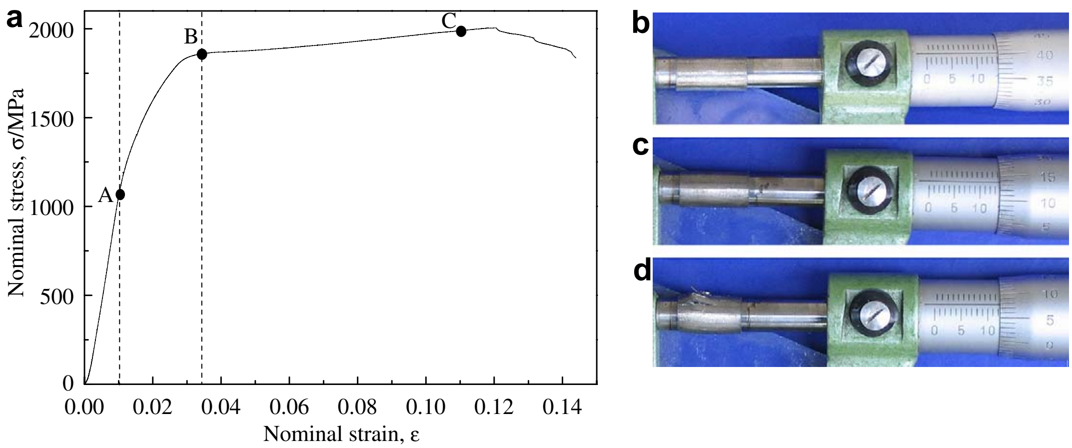

Fig. 5. W–BMG composite appearances during quasi-static compressive deformation. (a) three deformation stages A, B and C, marked in quasi-static stress–strain curve; (b), (c) and (d) appearances of the W–BMG composite deformed in stages A, B and C.

are visible in the BMG matrix, forming a chap pattern as shown in Fig. 6. In stage C, where the stress is close to the maximum yielding stress, buckling occurs in the tungsten wires [see Fig. 5(d)]. It is conjectured that the yielding plateau is a buckling process of the tungsten wires which result in the weak strain hardening.

The appearances of the W-BMG composite samples deformed upon both quasi-static and dynamic loads are shown in Fig. 7. It can be seen that the tungsten wires in the composite subjected to quasi-static load show a serious buckling deformation until breakdown [see Fig. 7(a)]. For dynamic load, the tungsten wires in the W-BMG composite exhibit s-type warping [see Fig. 7(b)]. Some longitudinal cracks appear on the surface of the composite sample. It can be rationally supposed that the stress plateau after the yield peak corresponds to the tungsten wires warping. The difference in damage behavior of the tungsten wires, i.e., the buckling and warping, is the possible reason resulting in the different plastic strains between the quasi-static deformation and dynamic deformation.

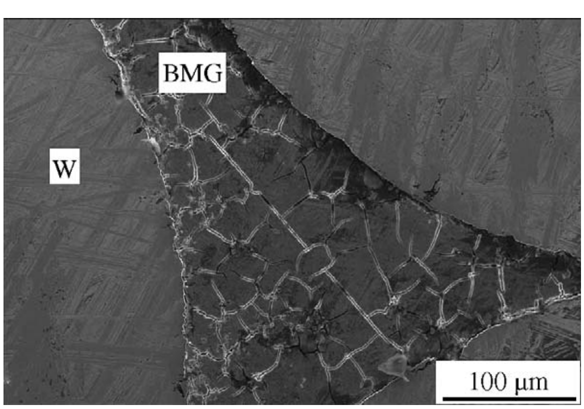

Fig. 6. SEM cross-section image of the W–BMG composite in stage B during quasi-static compressive deformation.

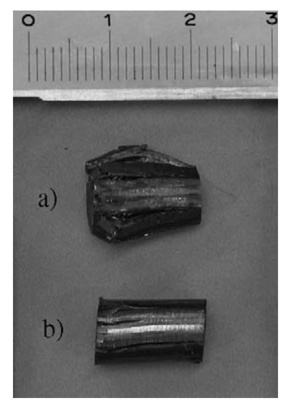

Fig. 7. Overview on the compressive deformation of W–BMG composites under various deformation conditions. (a) quasi-static deformation; (b) dynamic deformation.

4. Discussions

In the elastic deformation stage both BMG matrix and tungsten wires behave as elastic materials. In this region the composite responds with increased elasticity due to the combined effect of the two metals. We calculate Young's modulus of the composite using the rule of mixtures:

$$E_c = E_m V_m + E_f V_f \cong 310\text{GPa}, \quad (1)$$

where E_m and E_f are Young's moduli of the BMG and tungsten, respectively ($E_m = 96$ GPa, $E_f = 410$ GPa, see Table 1); V_m and V_f are their volume fractions. This calculation is corroborated by the stress–strain results shown in Fig. 3. When the load is removed, the dimensions of the W-BMG composite almost return to their original values [cf. Fig. 5(b)].

For the strain hardening deformation stage [from A to B, see Fig. 5(a)], we must consider the effects involved in fabricating the composite samples and the resulting frozen-in stresses due to differential thermal shrinkage. To calculate the frozen-in stresses, we assume that on cooling from the infiltration temperature the composite becomes

Table 1
Physical properties of the BMG and tungsten [11]

	Tungsten	$Zr_{41.25}Ti_{13.75}Ni_{10}Cu_{12.5}Be_{22.5}$ BMG
Poisson's ratio, υ	0.28	0.36
Ultimate strength, σ_b (MPa)	2350	1880
Tensile yield strength, σ_y (MPa)	1700	1817
Tensile strain to fracture, ε	0.019	0.02
Thermal expansion coefficient, α (10^{-6}/K)	4.5	8.5
Young's modulus, E (GPa)	410	96

a unified solid at the glass transition temperature of the BMG. If it is cooled further down to room temperature, the two adherent metallic phases, with different thermal expansion coefficients, experience different thermal shrinkage rates (see Table 1). To estimate the magnitude of the frozen-in stresses, we proceed as follows:

(1) First, assume that the BMG matrix and the tungsten wires are not adhering to each other. Then the lengthwise contraction and final length in the BMG matrix is given by:

$$\Delta L_m = L_{T_g} \times \alpha_m \times \Delta T \to L_m = L_{T_g}[1 - \alpha_m \Delta T], \quad (2)$$

and the corresponding thermal shrinkage in the tungsten wires is:

$$\Delta L_f = L_{T_g} \times \alpha_f \times \Delta T \to L_f = L_{T_g}[1 - \alpha_f \Delta T], \quad (3)$$

where L_{T_g} is the length of the composite sample at the glass transition temperature; L_m and L_f are respectively the lengths of the BMG matrix and the tungsten wires at room temperature under the assumption of free shrinkage (no adhesion); α_m and α_f are the thermal expansion coefficients of the BMG matrix and tungsten, respectively. Assuming that $\Delta T = 380$ K for the temperature difference [11] and using the values of the coefficients of thermal expansion in Table 1, the ratio R is estimated as:

$$R = \frac{L_m}{L_f} = \frac{1 - \alpha_m \Delta T}{1 - \alpha_f \Delta T} = 0.998. \quad (4)$$

(2) Next, apply longitudinal forces, F'_m and F'_f, to the BMG matrix and the tungsten wires, respectively, such that:

$$L'_m = L'_f, \quad (5)$$

where L'_m and L'_f are the new lengths of BMG matrix and the tungsten wires, respectively. Then the strains in the BMG matrix and the tungsten wires are given by:

$$\begin{cases} \varepsilon_m = (L_m - L'_m)/L_m \\ \varepsilon_f = (L_f - L'_f)/L_f \end{cases}. \quad (6)$$

(3) Now, the matrix and the wires are made to adhere, and the external forces are removed. The two phases react against each other, and reach equilibrium when:

$$-\sigma_m V_m = \sigma_f V_f, \quad (7)$$

where σ_m and σ_f are the stresses in the BMG matrix and the tungsten wire phase, respectively, and V_m and V_f are the corresponding area (volume) fractions. Using Hooke's law, the following relationships can be derived for the strains:

$$\begin{cases} \varepsilon_m = \frac{E_m + E_f(V_f/V_m)}{E_m + E_f(V_f/V_m)R} - 1, \\ \varepsilon_f = \frac{E_f + E_m(V_m/V_f)}{E_f + E_m(V_m/V_f)(1/R)} - 1. \end{cases} \quad (8)$$

Taking the appropriate values from Table 1, and noting that $V_m + V_f = 1$, the strains are calculated as below:

$$\begin{cases} \varepsilon_m = 1.80 \times 10^{-3}, \\ \varepsilon_f = -1.98 \times 10^{-4}. \end{cases} \quad (9)$$

(4) Finally, Assuming these values to be the strains in the composite samples when cooling from glass transition temperature to room temperature, the corresponding frozen-in stresses are obtained:

$$\begin{cases} \sigma_m = E_m \varepsilon_m \cong 173 \text{ MPa}, \\ \sigma_f = E_f \varepsilon_f \cong -81.2 \text{ MPa}. \end{cases} \quad (10)$$

The calculation shows that the matrix contains tensile frozen-in stresses and the wires are subjected to compressive frozen-in stresses in the longitudinal direction. The above calculation does not take into account any relaxation of the stresses in the matrix or any interfacial slip between the BMG matrix and the tungsten wires.

It is more difficult to calculate the frozen-in stresses and strains in the transverse direction due to the complexity of the microstructure. As is evident in Fig. 2(a), the tungsten wires are essentially in contact with each other, so the isolated pools of the BMG matrix are confined and restricted. Differential thermal shrinkage should result in transverse, tensile frozen-in stresses in the matrix of a magnitude which is similar to that calculated above for the longitudinal direction. Therefore, the BMG matrix appears to be in a state of tri-axial tension. The adhesion between the matrix and the wires appears to be strong enough so that no decohesion is observed at the interface [Fig. 2(b)].

As the W–BMG composite is subjected to a uniaxial compression, the first sign of non-linear behavior appears at a stress level being approximately a half of the compressive strength. In this deformation stage (from A to B), cracking in the BMG matrix (cf. Fig. 6) suggests that slight barrelling of the specimens occurs although buckling of tungsten wires in the macroscale cannot be observed. Plasticity in monolithic BMG is very limited (cf. Fig. 3). In view of these observations, our interpretation of the stress–strain behavior in the stage from A to B is as follows. When the stress level reaches point A, most of the compressive load is carried by the tungsten wires because of its higher volume fraction (68%), higher elastic modulus, and also because of the existence of the compressive frozen-in stress (−81.2 MPa) as opposed to the tensile stress in the matrix (173 MPa). The calculated buckling stress for tungsten wire, assuming the wires having unrestricted, freely rotatable ends, is estimated from Euler's formula:

$$\sigma_{cr} = \frac{\pi^2}{16} \times \frac{E_f d_f^2}{L_f^2} \cong 1300 \text{ MPa}. \tag{11}$$

The outer wires in the composite are not supported laterally and therefore they may start buckling at or around point A of Fig. 3, at which the value of stress is lower than σ_{cr}. After the wires are buckled, the BMG matrix should be squeezed and some cracks appear (cf. Fig. 6), which in turn relieves stress and weakens lateral support for the next layer of wires. As such, the stress does not linearly increase with strain in the A–B region. In contrast, the wires close to the center of the W–BMG composite are fully supported by the BMG matrix and require much higher buckling load to give way even though the crack appears on this BMG matrix. Therefore, the stress increases to a level of 1871 MPa, i.e. point B of Fig. 3, in which the decreasing load carried by the buckled wires balance the increasing load carried by the as yet un-buckled wires. The outer ring of damage is gradually growing towards the center, finally reaching its limits at a strain of approximately 0.14 [cf. Fig. 5(a)], beyond which a total collapse and disintegration of the composite occur.

It can be assumed that the dynamic compression of the W–BMG composite by the SHPB method follows a similar deformation and damage process, although dynamic strain rate may affect the deformation behavior. The buckling appears to be of a different mode, and the flow stress reaches much higher values.

To further discuss the influence of the strain rate on the deformation behavior of the W–BMG composite, a strain rate sensitivity exponent is introduced, which can be expressed by a power law relation [24]:

$$\frac{\sigma}{\sigma_0} = \left(\frac{\dot{\varepsilon}}{\dot{\varepsilon}_0}\right)^m, \tag{12}$$

where σ is the flow stress at a selected strain rate which is the maximum bearing stress under dynamic condition; σ_0 is the stress at a reference strain rate which is taken here to be the maximum bearing stress for a particular quasi-static load; m is the strain rate sensitivity exponent, $\dot{\varepsilon}$ is the strain rate and $\dot{\varepsilon}_0$ is the reference strain rate which is the quasi-static strain rate in present study. According to Eq. (12), the logarithm of flow stress is expected to be linearly dependent on the logarithm of strain rate, as shown in Fig. 8. By linear regression, the strain rate sensitivity exponent is estimated to be 0.022 (see Fig. 8). The strain rate sensitivity exponent of the tungsten was found to be 0.042 in an earlier study [25,26]. Since Subhash et al. [27] have proved that the monolithic BMG had fracture strength insensitive to a strain rate, it can be proposed that a change in mechanical properties of the tungsten wires is the main factor affecting the deformation behavior of the composite upon dynamic load. Strain rate sensitivity exponent is a parameter inversely proportional to the flow stress of the material subjected to dynamic load [28,29]. In general, decreasing in the value of the strain rate sensitivity exponent indicates an increase in the flow stress [28]. In the present study, the damage of the W–BMG composite under dynamic load shows warping of the tungsten wires rather than fracture of the tungsten wires. In this case, confining of the isolated pools of the BMG matrix and toughing of the neighboring tungsten wires are important factors resulting in the strain rate sensitivity exponent. Although the frozen-in stresses and strains in the transverse direction of the W–BMG composite cannot be found, according to a coaxial cylinder model as discussed in Refs. [11,30,31], the tungsten wires should be subjected to a frozen-in hoop stress. This hoop stress can restrict the buckling or warping of the tungsten wires and promotes the flow stress of the tungsten wires. Increase in the flow stress reduces the strain rate sensitivity exponent of the tungsten. Therefore, the W–BMG composite shows a smaller strain rate sensitivity exponent of 0.022 as compared with that of the monolithic tungsten.

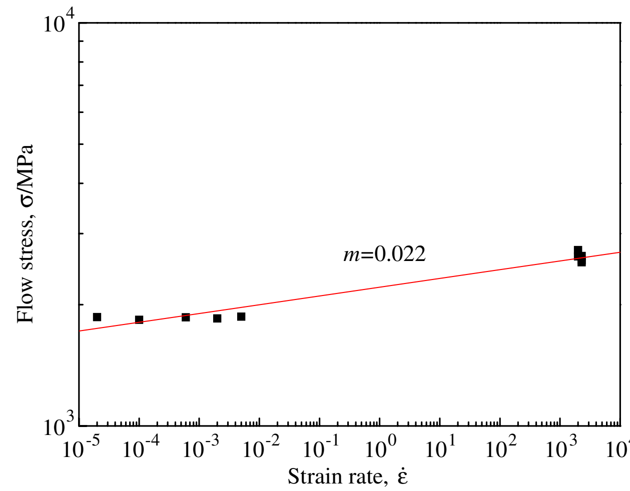

Fig. 8. Strain rate sensitivity exponent of the W–BMG composite.

5. Conclusions

(1) Compared with the monolithic BMG, the tungsten wires reinforced BMG composite shows a higher plastic strain of 0.14 but the lower yield stress of 1087 MPa upon quasi-static load. The tungsten does not evidently improve the compressive stress (1871 MPa) of the composite. The stress–strain behavior of the W–BMG composite can be divided into three stages, i.e., elastic deformation stage, strain hardening deformation stage and plastic deformation stage. In the elastic deformation stage, the BMG matrix and the tungsten wires exhibit elastic deformation behavior. In the strain hardening deformation stage, some of the tungsten wires commence buckling, which squeezes the BMG matrix. The cracked BMG matrix constraints the tungsten wires, promoting the stress level. In the plastic deformation stage, a large strain prior to failure can be

achieved as a result of buckling of most of the tungsten wires.

(2) In the dynamic compressive deformation, the compressive stress of the W–BMG composite is as high as 2700 MPa, which is 1.4 times that found under quasi-static condition. The strain rate sensitivity exponent of the W–BMG composite is measured to be 0.022, which is half of that of monolithic tungsten. The lower strain rate sensitivity of the composite is due to the frozen-in stress.

Acknowledgements

This work was supported by the Program for New Century Excellent Talents in University (China). The assistance from staff members in the Electron Microscope Unit at the Australian National University is acknowledged.

References

[1] A. Inoue, B.L. Shen, H. Koshiba, H. Kato, A.R. Yavari, Nature Mater. 2 (2003) 661.
[2] J. Shen, Q.J. Chen, J.F. Sun, H.B. Fan, G. Wang, Appl. Phys. Lett. 86 (2005) 151907.
[3] M. Stoica, J. Eckert, S. Roth, Z.F. Zhang, L. Schultz, W.H. Wang, Intermetallics 13 (2005) 764.
[4] X.K. Xi, D.Q. Zhao, M.X. Pan, W.H. Wang, Y. Wu, J.J. Lewandowski, Phys. Rev. Lett. 94 (2005) 125510.
[5] Z. Bian, H. Kato, C.L. Qin, W. Zhang, A. Inoue, Acta Mater. 53 (2005) 2037.
[6] R.D. Conner, R.B. Dandliker, V. Scruggs, W.L. Johnson, Inter. J. Impact Eng. 24 (2000) 435.
[7] C.-Y. Haein, J. Schroers, W.L. Johnson, Appl. Phys. Lett. 80 (2002) 1906.
[8] B. Clausen, S.-Y. Lee, E. Üstündag, C.C. Aydiner, R.D. Conner, M.A.M. Bourke, Scripta Mater. 49 (2003) 123.
[9] D. Dragoi, E. Üstündag, B. Clausen, M.A.M. Bourke, Scripta Mater. 45 (2001) 245.
[10] K.Q. Qiu, A.M. Wang, H.F. Zhang, B.Z. Ding, Z.Q. Hu, Intermetalllics 10 (2002) 1283.
[11] R.D. Conner, R.B. Dandliker, W.L. Johnson, Acta Mater. 40 (1998) 6089.
[12] Y.-L. Huang, A. Bracchi, T. Niermann, M. Seibt, D. Danilov, B. Nestler, S. Schneider, Scripta Mater. 53 (2005) 93.
[13] W. Löser, J. Das, A. Güth, H.-J. Klauß, C. Mickel, U. Kühn, J. Eckert, S.K. Roy, L. Schultz, Intermetallics 12 (2004) 1153.
[14] G. Wang, J. Shen, J.F. Sun, Z.P. Lu, Z.H. Stachurski, B.D. Zhou, Intermetallics 13 (2005) 642.
[15] A. Peker, W.L. Johnson, Appl. Phys. Lett. 63 (1993) 2342.
[16] C.-Y. Haein, R.D. Conner, F. Szuecs, W.L. Johnson, Scripta Mater. 45 (2001) 1039.
[17] J.M. Staehler, W.W. Predebon, B.J. Pletka, J. Lankford, J. Am. Ceram. Soc. 76 (1993) 536.
[18] M. Guden, I.W. Hall, Mater. Sci. Eng. A 232 (1997) 1.
[19] L.D. Oosterkamp, A. Ivankovic, G. Venizelos, Mater. Sci. Eng. A 278 (2000) 225.
[20] G. Ravichandran, G. Subhash, J. Am. Ceram. Soc. 77 (1994) 263.
[21] H.A. Bruck, A.J. Rosakis, W.L. Johnson, J. Mater. Res. 11 (1996) 503.
[22] R.B. Dandliker, R.D. Conner, W.L. Johnson, J. Mater. Res. 13 (1998) 2896.
[23] G. Wang, J. Shen, J.F. Sun, B.D. Zhou, J.D. Fitz Gerald, D.J. Llewellyn, Z.H. Stachurski, Scripta Mater. 53 (2005) 641.
[24] Q. Wei, T. Jiao, S.N. Mathaudhu, E. Ma, K.T. Hartwig, K.T. Ramesh, Mater. Sci. Eng. A 358 (2003) 266.
[25] J.H. Bechtold, P.G. Shewmon, Trans. ASME 46 (1954) 397.
[26] J.H. Bechtold, Trans. ASME 206 (1956) 142.
[27] G. Subhash, R.J. Dowding, L.J. Kecskes, Mater. Sci. Eng. A 334 (2002) 33.
[28] Q. Wei, K.T. Ramesh, E. Ma, L.J. Kesckes, R.J. Dowding, V.U. Kazykhanov, R.Z. Valiev, Appl. Phys. Lett. 86 (2005) 101907.
[29] D. Caillard, J.L. Martin, Thermally Activated Mechanisms in Crystal Plasticity, Pergamon, Amsterdam, 2003, p. 13.
[30] T.W. Clyne, P.J. Withers, An Introduction to Metal Matrix Composites, Cambridge University, Cambridge, 1993, p. 12, 30, 108.
[31] Y. Mikata, M. Taya, J. Comp. Mater. 19 (1985) 554.